Available online at www.sciencedirect.com
ScienceDirect
Journal of Computational Physics 225 (2007) 183–205
JOURNAL OF COMPUTATIONAL PHYSICS
www.elsevier.com/locate/jcp

A level set approach to anisotropic flows with curvature regularization

Martin Burger [a], Frank Haußer [b,*], Christina Stöcker [b], Axel Voigt [b,c]

[a] *Institut für Numerische und Angewandte Mathematik, Westfälische Wilhelms-Universität Münster, Einsteinstrasse 62, 48149 Münster, Germany*
[b] *Crystal Growth group, Research Center Caesar, Ludwig-Erhard-Allee 2, 53175 Bonn, Germany*
[c] *Institut für Wissenschaftliches Rechnen, Technische Universität Dresden, Zellescher Weg 12-14, 01069 Dresden, Germany*

Received 5 January 2006; received in revised form 6 November 2006; accepted 23 November 2006
Available online 16 January 2007

Abstract

Modeling and simulation of faceting effects on surfaces are topics of growing importance in modern nanotechnology. Such effects pose various theoretical and computational challenges, since they are caused by non-convex surface energies, which lead to ill-posed evolution equations for the surfaces. In order to overcome the ill-posedness, regularization of the energy by a curvature-dependent term has become a standard approach, which seems to be related to the actual physics, too. The use of curvature-dependent energies yields higher order partial differential equations for surface variables, whose numerical solution is a very challenging task.

In this paper, we investigate the numerical simulation of anisotropic growth with curvature-dependent energy by level set methods, which yield flexible and robust surface representations. We consider the two dominating growth modes, namely attachment–detachment kinetics and surface diffusion. The level set formulations are given in terms of metric gradient flows, which are discretized by finite element methods in space and in a semi-implicit way as local variational problems in time. Finally, the constructed level set methods are applied to the simulation of faceting of embedded surfaces and thin films.

PACS: 02.30.Zz; 02.60.Pn; 02.60.Lj

Keywords: Anisotropic surface growth; Curvature regularization; Faceting; Level set methods; Higher-order geometric flows

1. Introduction

In this paper, we develop level set methods for the simulation of faceted growth of surfaces. The underlying models are anisotropic geometric evolution laws either based on attachment–detachment or on surface diffusion mechanisms. Both types of evolutions are driven by the chemical potential, which arises as the variation

* Corresponding author.
E-mail addresses: martin.burger@uni-muenster.de (M. Burger), hausser@caesar.de (F. Haußer), stoecker@caesar.de (C. Stöcker), voigt@caesar.de (A. Voigt).

0021-9991/$ - see front matter © 2006 Elsevier Inc. All rights reserved.
doi:10.1016/j.jcp.2006.11.026

of the surface energy. The form of the latter is a key issue for modeling faceting: In order to obtain faceting effects, the surface free energy is usually determined as a non-convex function of the normal orientation, which creates preferred directions in the equilibria (facets).

The non-convexity of the surface energy leads to backward diffusion effects and consequently ill-posedness of the evolution equations. In order to regularize these problems, higher order expansions of the energies are carried out, which lead to terms depending on curvature. For the corresponding evolution equations this yields higher order differential operators and additional nonlinearities, which are difficult to analyze and to simulate numerically. In this paper, we shall construct stable methods based on level set representations of the surfaces, spatial discretizations by finite element methods and semi-implicit time discretizations.

The paper is organized as follows: In the remaining parts of the introduction, we provide a motivation for the problems under investigation, before we discuss equilibrium situations and the type of energy needed to model faceting. The latter is the key ingredient for the formulation of the geometric evolution laws, which we also provide in the introduction. In Section 2, we derive level set formulations for the geometric evolution laws, which are given in terms of metric gradient flows. As a consequence of the latter, local-in-time variational problems can be derived to approximate the flow, and they are used to construct discrete approximations (in space and time) in Section 3. Implementation aspects are discussed in Section 4, before we give various numerical examples in Section 5.

1.1. Thin film growth

To understand or even control the evolution of the surface morphology of a growing crystalline film is a key ingredient for several applications on a nanometer length scale. Mound formation in epitaxially grown films for example has been attracting wide attention over the last years due to its role in the self-organized evolution of quantum dots, where the goal is to produce regular structures of nano-mounds in a bottom-up approach. In other applications one might be more interested in preventing such mound formation. In a top-down approach to produce nanostructures for novel electronic devices the goal is to produce a homogeneous almost flat surface. What in the end determines the surface morphology is a complicated competition between several effects, including strong anisotropies in the surface free energy [42,28], elastic stress caused by a lattice misfit between the crystalline film and the substrate [36], kinetic anisotropic surface fluxes resulting from energy barriers [38,39], effects due to intermixing [45] and probably many more. We will concentrate on the effect of faceting (spinodal decomposition) of thermodynamically unstable crystal surfaces caused by strong anisotropic surface free energy densities and will leave the incorporation of other effects to future investigations. Moreover, we will not consider growth, but rather study annealing of surfaces. To understand the atomistic rearrangement upon annealing in the evolution towards the equilibrium, we first summarize results on the equilibrium crystal shape, which is expected to form the long-time asymptotic of the flows we shall consider in this paper.

1.2. Equilibrium crystal shape

To determine the shape of a crystal in equilibrium is a classic problem in materials science, dating back to Herring [26]. Given a surface free energy density γ, the equilibrium shape (''Wulff shape'') is defined as the shape of minimum surface free energy $e[\Sigma] = \int_\Sigma \gamma$ under the constraint of fixed volume. Usually, $\gamma = \gamma(n)$ is assumed to be a function of the local orientation n of the crystal surface, reflecting the crystal anisotropy. Moreover, γ depends on the temperature. While at zero temperature 0 K the equilibrium shape is perfectly faceted, above a certain material dependent temperature facets start to be separated by rough, rounded regions, which was recently demonstrated experimentally (cf. e.g. [44]). Facets may result from cusps in the surface free energy, which are blunted for increasing temperature making the facets shrink if the temperature is raised. However, facets may also arise from smooth but non-convex surface free energies as follows: the non-convexity of the free energy leads to missing orientations, i.e. sharp edges and corners in the Wulff-shape, since it is energetically favorable to exclude high energy orientations. In the case of closed surfaces, these edges/corners are connected by smooth surfaces with small curvature while in the case of a crystalline film the edges/corners are connected by facets.

To obtain rounded corners and edges, a free energy density $\hat{\gamma} = \hat{\gamma}(n, h, \ldots)$, with higher order terms is needed, where h is the mean curvature of the surface. An explicit form for $\hat{\gamma}$ has been introduced first for two-dimensional crystals by DiCarlo, Gurtin and Podio-Guidugli [17] and later for three-dimensional crystals by Jabbour and Gurtin [27], see also Rätz and Voigt [34]. Here we will follow [34] and consider a surface free energy of the form

$$e[\Sigma] = \int_\Sigma \left(\gamma(n) + \frac{\epsilon^2}{2} h^2\right) \mathrm{d}\sigma \tag{1}$$

with $\epsilon = \epsilon(T)$ introducing the length scale over which the corner/edge is rounded. A physical motivation for the regularizing term is to assume that regions of very high curvature (sharp corners/edges) have an additional contribution to the surface free energy. The effect of the higher order term on the Wulff shape can be understood as follows: An edge or a corner with large mean curvature has a high energy because of the second term in (1), while an edge or a corner with small mean curvature has a high energy because of a resulting large area with unprefered orientations in the first term. The amount of the rounding of edges and corners is thus a compromise between these two competing terms. The resulting equilibrium shapes have been analyzed in detail by Spencer [41] for two-dimensional crystals and the used asymptotic analysis may in principle also be applied to the three-dimensional setting. Much less understood is the dynamic behavior of the crystal shape if the surface free energy is given by (1). Note, that the energy (1) is the sum of the weighted area and the Willmore energy.

1.3. Geometric evolution equations

A common approach to derive an evolution equation for a crystal surface Σ is to consider as the driving force the surface chemical potential μ, which is the rate of change of the free energy, when moving the surface. Taking a variational approach, μ can be defined as the first variation of the surface free energy $e[\Sigma]$ with respect to normal variations of Σ, i.e. $\mu = \frac{\delta e}{\delta \Sigma}$, where we assume, that there is no contribution to μ from the bulk phases. In the case of attachment–detachment kinetics, the normal velocity v is taken to be proportional to μ

$$\beta v = -\mu,$$

with β being a kinetic coefficient. If the dynamics is assumed to be diffusion dominated, the surface flux is defined via the tangential gradient of the chemical potential as $v\nabla_\sigma \mu$, v being a mobility tensor for diffusion along the surface, leading to the continuity equation

$$v = \nabla_\sigma (v \nabla_\sigma \mu)$$

see [29,30]. For a detailed physical derivation of these evolution laws as the limit of a diffusion equation including free adatoms on the surface, we refer to [21].

Computing the chemical potential $\mu = \frac{\delta e}{\delta \Sigma}$ with the surface energy given in (1) leads to

$$\beta v = -h_\gamma + \epsilon^2 \left(\Delta_\sigma h + h\left(\|S\|^2 - \frac{1}{2} h^2\right)\right) \tag{2}$$

$$v = \nabla_\sigma \cdot \left(v \nabla_\sigma \left(h_\gamma - \epsilon^2 \left(\Delta_\sigma h + h\left(\|S\|^2 - \frac{1}{2} h^2\right)\right)\right)\right) \tag{3}$$

for the case of attachment–detachment dynamics and surface diffusion, respectively. Here Δ_σ is the surface Laplacian and $S = \nabla_\sigma n$ the shape operator with Frobenius norm $\|S\| = \sqrt{\mathrm{trace}(SS^{\mathrm{T}})}$. Moreover h_γ denotes the weighted mean curvature, which is defined through $h_\gamma = \nabla_\sigma \cdot n_\gamma$, with $n_\gamma = D\gamma(n)$ being the Cahn–Hoffmann vector on Σ. In the isotropic case, $\gamma(n) = 1$, we obtain $h_\gamma = h$. Obviously, setting $\epsilon = 0$, (2) reduces to anisotropic mean curvature flow and (3) to anisotropic surface diffusion. However, for non-convex surface free energies, these equations are ill-posed, i.e. backward parabolic for the missing orientations. Thus the higher order term introduced in the energy (1) can also be understood as a mathematical regularization of the ill-posed equations.

So far, there are no analytical results known for these highly nonlinear evolution laws and numerical treatments of these equations are also rare. In a two-dimensional setting (2) and (3) are solved by parametric finite elements in [24] and [23], respectively, and an approach based on complex methods is introduced in [37]. The latter approach is intrinsically two-dimensional. The methods used in [24,23] are based on the work of [7], where a discretization of parametric isotropic surface diffusion is introduced also for three dimensional surfaces. Extending this approach to the anisotropic case, as in [25], and combining it with the proposed discretization for Willmore flow in [35] may lead to a parametric finite element method also in three dimensions. However, due to the expected faceting of the surface and the appearance of regions with large curvature such a method most likely will result in severe problems for the regularity of the surface grid. Therefore, for a three-dimensional setting only methods which circumvent a direct triangulation of the evolving surface are appropriate. Eq. (3) is solved in a graph formulation in [9]. Furthermore several attempts have been made within a phase-field approximation. A model is proposed in [33], which incorporates a phase-field approximation for Willmore flow suggested in [19]. A slightly different phase-field model, which only takes approximations of the $\Delta_\sigma h$ term in the regularization into account, was used in [48]. A matched asymptotic analysis for both models, showing a formal convergence towards (3) is lacking so far. In this paper, we will consider a level set approach for (2) and (3), which circumvents the above mentioned difficulties and works for curves and for surfaces.

1.4. Level set methods for anisotropic geometric evolution equations

Level set methods for geometric evolution equations have already been discussed and applied numerically in the literature. For isotropic mean curvature flow and isotropic surface diffusion we refer for example to [40,16] and [12,40], respectively. In [13], a level set method for anisotropic mean curvature flow and surface diffusion has been introduced. However, these methods are restricted to convex surface energies, where no regularizing term in the surface energy is needed ($\epsilon = 0$). A level-set treatment for anisotropic geometric evolution equations with missing orientations has not yet been performed for neither of the equations. A level-set method for Willmore flow was introduced recently in [18]. In this work, we will derive level set methods for (2) and (3) in the spirit of [18,13].

2. Level set formulation of the models

In this section, we discuss the level set formulation of the curvature regularized anisotropic motions by mean curvature and by surface diffusion. Both of them can be formulated as gradient flows for the same energy, and therefore we discuss the properties and reformulation of the energy before specifying the special evolution models.

2.1. Level set formulation

We start by fixing the basic notations needed for the level set formulations below, a detailed discussion of level set methods can be found in [32,31]. Let $\Sigma(t) \subset \Omega \subset \mathbb{R}^d$ be an evolving curve or surface, such that

$$\Sigma(t) = \partial\Theta(t) \setminus \partial\Omega.$$

We assume that the curve or surface either lies in the interior of the domain Ω or – in the case of periodic boundary condition – is periodic. Moreover we will be concerned with connected embedded curves or surfaces only. However, also disconnected curves/surfaces and topological changes could be treated in the presented framework. Because in the application of interest topological changes are not of relevance, we do not consider this situation in detail. The level set approach amounts to choosing a function $\phi : \Omega \times \mathbb{R} \to \mathbb{R}$ such that

$$\Sigma(t) = \{\phi(.,t) = 0\}, \quad \Theta(t) = \{\phi(.,t) < 0\}.$$

It is straightforward (cf. e.g. [31]) to see that the unit normal vector n (pointing into $\Omega \setminus \Theta(t)$), the normal velocity v, and the mean curvature h of the evolving surface can be represented as

$$n = \frac{\nabla\phi}{|\nabla\phi|}, \quad v = -\frac{\partial_t\phi}{|\nabla\phi|}, \quad h = \nabla\cdot\left(\frac{\nabla\phi}{|\nabla\phi|}\right), \tag{4}$$

where we assume that $\nabla\phi$ does not vanish. Note that with this sign convention a closed sphere with outer normal n has positive mean curvature $h > 0$. For simplicity we assume in the following natural boundary conditions for ϕ. The case of periodic boundary condition may be treated in the same manner.

2.2. Energy and chemical potential

Recall the curvature regularized energy of a surface Σ given in (1)

$$e[\Sigma] = \int_\Sigma \left(\gamma(n) + \frac{\epsilon^2}{2}h^2\right) \mathrm{d}\sigma, \tag{5}$$

with n and h denoting the normal and mean curvature as above, and $\gamma : \mathbb{R}^d \to \mathbb{R}$ being a positive one-homogeneous anisotropy function. As in [18], in order to obtain a level set formulation we extend the energy to arbitrary level sets of ϕ (assuming sufficient regularity and that $\nabla\phi$ does not vanish on a set of positive measure) and then average over the levels, i.e.

$$E[\phi] := \int_{\mathbb{R}} \int_{\Sigma^\alpha} \left(\gamma(n) + \frac{\epsilon^2}{2}h^2\right) \mathrm{d}\sigma\,\mathrm{d}\alpha,$$

where $\Sigma^\alpha := \{\phi = \alpha\} \cap \Omega$. Using the level set representation of the normal vector, the co-area formula [20,3], and the homogeneity of γ, the averaged energy can be rewritten as

$$E[\phi] = \int_\Omega \left(\gamma(\nabla\phi) + \frac{\epsilon^2}{2}|\nabla\phi|H^2\right) \mathrm{d}x, \tag{6}$$

where H denotes the extension of the mean curvature of the level sets, now interpreted as a function on Ω. The definition of the mean curvature can be reformulated in weak form as

$$\int_\Omega H\vartheta\,\mathrm{d}x = -\int_\Omega \frac{\nabla\phi\cdot\nabla\vartheta}{|\nabla\phi|}\,\mathrm{d}x \tag{7}$$

for all sufficiently smooth test functions $\vartheta \in H_0^1\Omega$.

The driving force of any evolution mode is the difference of the chemical potential μ from its equilibrium value. Since the chemical potential can be computed as the variation of the energy for local surface perturbations in normal direction, it will be our next task to compute energy variations. The variations in normal directions can be computed easily from the level set representation in a weak form, namely as

$$\int_\Omega \mu\eta\,\mathrm{d}x = -E'[\phi]\eta$$

for all smooth test functions η (note the negative sign caused by $E'[\phi] \sim -e'[\Sigma]$ in our sign convention). In order to simplify this analysis with respect to the mean curvature we use a Lagrangian formulation of the constraint (7), i.e. we introduce a dual variable ω to obtain

$$L[\phi, H, \omega] = \int_\Omega \left(\gamma(\nabla\phi) + \frac{\epsilon^2}{2}|\nabla\phi|H^2 + \epsilon^2 H\omega + \epsilon^2\frac{\nabla\phi\cdot\nabla\omega}{|\nabla\phi|}\right)\mathrm{d}x. \tag{8}$$

As well-known in the context of PDE-constrained optimization problems (see e.g. [22]) one obtains the energy variation and thus the chemical potential as

$$-\int_\Omega \mu\eta\,\mathrm{d}x = \partial_\phi L(\phi, H, \omega)\eta \tag{9}$$

$$= \int_\Omega \left(\gamma_z(\nabla\phi)\cdot\nabla\eta + \frac{\epsilon^2}{2}\frac{\nabla\phi\cdot\nabla\eta}{|\nabla\phi|}H^2 + \epsilon^2\frac{\nabla\eta\cdot(\mathbf{P}\nabla\omega)}{|\nabla\phi|}\right)\mathrm{d}x \tag{10}$$

for H and ω satisfying

$$0 = \partial_H L[\phi, H, \omega]\psi = \epsilon^2 \int_\Omega (H|\nabla\phi|\psi + \psi\omega)\,\mathrm{d}x \tag{11}$$

$$0 = \partial_\omega L[\phi, H, \omega]\vartheta = \epsilon^2 \int_\Omega \left(H\vartheta + \frac{\nabla\phi\cdot\nabla\vartheta}{|\nabla\phi|}\right)\mathrm{d}x \tag{12}$$

for all test functions η, ψ, and ϑ. Here we have used the notation

$$\mathbf{P} := \mathbf{I} - \frac{\nabla\phi}{|\nabla\phi|}\otimes\frac{\nabla\phi}{|\nabla\phi|} \tag{13}$$

for the projection matrix $\mathbf{P}$ and $\gamma_z(n) := D\gamma(n)$, where $D\gamma$ is the differential of the one-homogeneous function γ. The relation for the derivative E' can be simplified by eliminating (11), which yields $\omega = -H|\nabla\phi|$ (since the test function ψ was arbitrary). This yields the equations

$$-\int_\Omega \mu\eta\,\mathrm{d}x = \int_\Omega \left(\gamma_z(\nabla\phi)\cdot\nabla\eta + \frac{\epsilon^2}{2}\frac{\nabla\phi\cdot\nabla\eta}{|\nabla\phi|^3}\omega^2 + \epsilon^2\frac{\nabla\eta\cdot(\mathbf{P}\nabla\omega)}{|\nabla\phi|}\right)\mathrm{d}x \tag{14}$$

$$\int_\Omega \frac{\omega\vartheta}{|\nabla\phi|}\,\mathrm{d}x = \int_\Omega \frac{\nabla\phi\cdot\nabla\vartheta}{|\nabla\phi|}\,\mathrm{d}x. \tag{15}$$

Note that after elimination of H in favor of ω, this corresponds to a saddle-point formulation for the Lagrangian

$$\Lambda[\phi,\omega] := L(\phi, H(\phi,\omega),\omega) = \int_\Omega \left(\gamma(\nabla\phi) - \frac{\epsilon^2}{2}\frac{\omega^2}{|\nabla\phi|} + \epsilon^2\frac{\nabla\phi\cdot\nabla\omega}{|\nabla\phi|}\right)\mathrm{d}x, \tag{16}$$

in particular we have

$$E[\phi] = \sup_\omega \Lambda(\phi,\omega).$$

We finally notice that the dual variable $\omega = -H|\nabla\phi|$ equals the *curvature concentration* used for the weak formulation of Willmore flow (where the energy consists of the curvature term only) in [18] and for the surface diffusion with graph representations in [9]. Note that opposed to earlier work, the curvature concentration arises in a natural way as the dual variable in the saddle-point formulation of the energy.

2.3. Gradient flow formulation

In the following, we recall the gradient flow formulation of evolutions, which will be of fundamental importance for the construction of time discretizations below. For this sake we need a generalization of the classical gradient flow concept in metric spaces (cf. [2]), restricting ourself to the case of a Riemannian manifold in the following. If d denotes a metric on a suitable class of shapes, then the metric gradient flow is obtained as the limit $\tau \to 0$ of the variational problems

$$\Sigma(t+\tau) = \arg\min_\Sigma \left\{\frac{1}{2\tau}d(\Sigma,\Sigma(t))^2 + e[\Sigma]\right\}. \tag{17}$$

For τ small one only expects small changes of the surface and therefore it is natural to expand around the previous time step in the form

$$\Sigma^{v,\tau}(t) = \{x + \tau v n | x \in \Sigma(t)\}, \tag{18}$$

where v is the normal velocity. For such approximations it turns out that the metric and energy can be expanded as

$$d(\Sigma^{v,\tau}(t),\Sigma(t))^2 = \tau^2 B_{\Sigma(t)}(v,v) + \mathcal{O}(\tau^3),$$

with a symmetric positive definite bilinear form $B_{\Sigma(t)}$ (depending on the last time step $\Sigma(t)$ and corresponding to the metric tensor). Minimizing (17) over surfaces of the form $\Sigma^{v,\tau}(t)$ can therefore be approximated to first-order in τ via the minimization

$$\min_v \left\{ \frac{\tau}{2} B_{\Sigma(t)}(v,v) + e[\Sigma^{v,\tau}(t)] \right\}. \tag{19}$$

For attachment–detachment dynamics the metric tensor is a functional of the normal velocities in the form (the L^2-metric)

$$B_{\Sigma(t)}(v,w) = \int_\Sigma \beta v w \, \mathrm{d}\sigma,$$

and for surface diffusion in the form (the H^{-1}-metric, cf. [11,1])

$$B_{\Sigma(t)}(v,w) = \int_\Sigma (v \nabla_\sigma \psi_v) \cdot \nabla \psi_w \, \mathrm{d}\sigma,$$

where

$$\nabla_\sigma \cdot (v \nabla_\sigma \psi_v) = v.$$

The level set formulation of the flow can now be obtained by averaging the metric tensor (i.e. the bilinear form $B_{\Sigma(t)}$) over level sets Σ^α of ϕ. Since the normal velocity is proportional to the time derivative of the level set functions ($\partial_t \phi = -v|\nabla\phi|$), this yields a bilinear form on time derivatives, which we shall denote by g_ϕ. With the above representation of the normal velocity and the co-area formula, we can average the L^2-metric to (with the functions $V = v|\nabla\phi|$ and $W = w|\nabla\phi|$)

$$g_\phi^2(V,W) = \int_{\mathbb{R}} \int_{\Sigma_\alpha} \beta v w \, \mathrm{d}\sigma \, \mathrm{d}\alpha = \int_\Omega \beta \frac{VW}{|\nabla\phi|^2} |\nabla\phi| \, \mathrm{d}x = \int_\Omega \beta \frac{VW}{|\nabla\phi|} \, \mathrm{d}x. \tag{20}$$

In a similar way, we can rewrite the H^{-1}-metric (with the projection matrix $\mathbf{P}$ as in Eq. (13)) as

$$g_\phi^{-1}(V,W) = \int_\Omega (v \mathbf{P} \nabla \psi_V) \cdot \nabla \psi_W |\nabla\phi| \, \mathrm{d}x, \tag{21}$$

where ψ_V satisfies

$$\nabla \cdot (v|\nabla\phi| \mathbf{P} \nabla \psi_V) = V.$$

Since $V = \tau^{-1}(\phi(t+\tau) - \phi(t))$ provides a first-order approximation of $\partial_t \phi$, the local optimization after averaging becomes

$$\phi(t+\tau) = \arg\min_\phi \left(\frac{1}{2\tau} g_{\phi(t)}(\phi - \phi(t), \phi - \phi(t)) + E[\phi] + \mathcal{O}(\tau) \right).$$

The minimizer has variation zero, and hence

$$\frac{1}{\tau} g_{\phi(t)}(\phi(t+\tau) - \phi(t), \vartheta) = -E'[\phi(t+\tau)]\vartheta + \mathcal{O}(\tau).$$

In the limit $\tau \to 0$ one obtains the weak formulation of the gradient flow

$$g_\phi(\partial_t \phi, \vartheta) = -E'[\phi]\vartheta, \tag{22}$$

for all test functions $\vartheta \in C_0^\infty(\Omega)$, which is often rewritten as

$$\partial_t \phi = -\mathrm{grad}_{g_\phi} E[\phi].$$

Below we shall show the coherence of the metric gradient flows with the level set formulation of the curvature regularized flows and use them to construct semi-implicit time discretizations.

2.4. Curvature regularized anisotropic mean curvature flow

From the above formula (4) of the normal velocity in level set form as well as (14) and (15) we deduce the level set formulation of the anisotropic mean curvature flow with curvature regularization given in (2):

$$\int_\Omega \beta \frac{\partial_t \phi \eta}{|\nabla \phi|}\,\mathrm{d}x = -\int_\Omega \left(\gamma_z(\nabla\phi)\cdot\nabla\eta + \frac{\epsilon^2}{2}\frac{\nabla\phi\cdot\nabla\eta}{|\nabla\phi|^3}\omega^2 + \epsilon^2\frac{\nabla\eta\cdot(\mathbf{P}\nabla\omega)}{|\nabla\phi|}\right)\mathrm{d}x \tag{23}$$

$$\int_\Omega \frac{\omega\vartheta}{|\nabla\phi|}\,\mathrm{d}x = \int_\Omega \frac{\nabla\phi\cdot\nabla\vartheta}{|\nabla\phi|}\,\mathrm{d}x. \tag{24}$$

for all test functions η and ϑ.

We mention that with the above definition of the bilinear functional g^2_ϕ and the chemical potential μ, the *curvature regularized anisotropic mean curvature flow* satisfies

$$g^2_\phi(\partial_t\phi,\eta) = \int_\Omega \mu\eta\,\mathrm{d}x = -E'[\phi]\eta,$$

i.e. (23) and (24) are the gradient flow in the L^2-metric.

2.5. Curvature regularized anisotropic surface diffusion

It is well-known for scalar mobility v (cf. [5,6,10]) that a divergence form differential operator involving only tangential derivatives can be rewritten in terms of the full gradient and the projection matrix $\mathbf{P}$ defined in (13) as

$$\nabla_\sigma\cdot(v\nabla_\sigma .) = \frac{1}{|\nabla\phi|}\nabla\cdot(v|\nabla\phi|\mathbf{P}\nabla .).$$

After transforming the diffusion equation for μ into level set form, we can obtain a standard weak formulation, and with (14), (15) we deduce the level set formulation for *curvature regularized anisotropic surface diffusion* given in (3):

$$\int_\Omega \partial_t\phi\psi\,\mathrm{d}x = \int_\Omega v(\mathbf{P}\nabla\mu)\cdot\nabla\psi|\nabla\phi|\,\mathrm{d}x \tag{25}$$

$$\int_\Omega \mu\eta\,\mathrm{d}x = -\int_\Omega \left(\gamma_z(\nabla\phi)\cdot\nabla\eta + \frac{\epsilon^2}{2}\frac{\nabla\phi\cdot\nabla\eta}{|\nabla\phi|^3}\omega^2 + \epsilon^2\frac{\nabla\eta\cdot(\mathbf{P}\nabla\omega)}{|\nabla\phi|}\right)\mathrm{d}x \tag{26}$$

$$\int_\Omega \frac{\omega\vartheta}{|\nabla\phi|}\,\mathrm{d}x = \int_\Omega \frac{\nabla\phi\cdot\nabla\vartheta}{|\nabla\phi|}\,\mathrm{d}x \tag{27}$$

for all test functions ψ, η and ϑ. It is a straight-forward calculation to verify, that

$$g^{-1}_\phi(\partial_t\phi,\eta) = \int_\Omega \mu\eta\,\mathrm{d}x = -E'[\phi]\eta,$$

i.e. (25)–(27) is the gradient flow in the H^{-1}-metric.

2.6. Local level set approach

It is worth noticing that in the case of E being a functional depending on higher than first derivatives, the "global" level set approach is not well-defined. In this case the resulting evolution equation is a partial differential equation of higher than second order, and therefore does not satisfy a comparison principle. Consequently, even if a solution to the equation for the level set function ϕ exists, one cannot guarantee that ϕ is continuous and that its level sets are still the boundary of the sublevel sets (due to possible intersection and annihilation of level sets). This means that the level set approach can only be interpreted in a local sense for the regularized geometric flows, i.e., the level set function only satisfies the partial differential equations at the zero level set. Since one is not really interested in the other level sets of ϕ, one can use an arbitrary extension such as the signed distance function. In a theoretical approach this means one looks for a solution ϕ, which satisfies the partial differential equation only on the implicitly defined set $\{\phi = 0\}$, and is a signed distance function in the remaining part of Ω.

In a computational method, the local level set approach is rather straight-forward to realize. One first computes one (small) time-step of the partial differential equation (i.e., one violates the constraint of being a signed-distance function) and then performs a re-distancing step (i.e., one computes a suitable projection to the constraint set of signed-distance functions). To make this approach work one just has to ensure that the first step does not yield a too large deviation from the constraint set, which yields a restriction of the time step size. The numerical computation of signed-distance functions, which one has to perform in this approach, is discussed in [43]. The algorithm used is an extension of the method proposed in [8] to dimension $d = 3$.

In practice, re-distancing after each time step is not necessary as long as ϕ remains close enough to signed-distance near the interface. In our implementation we make use of re-distancing when the gradient of ϕ violates too much the signed-distance condition near the interface, i.e. when the norm of the gradient of ϕ deviates too much from $|\nabla\phi| = 1$ (see Section 5).

3. Discretization

In the following, we discuss the discretization of the regularized anisotropic flows introduced above. We mention again that due to the missing maximum principle these discretizations have to be interpreted in a local way, i.e., after computing one (sufficiently small) time step of the level set equation we will perform a re-distancing step.

3.1. Spatial semi-discretization by finite elements

We start with a spatial semi-discretization based on finite element methods. This choice seems natural due to the dissipative structure of the flows and the available weak formulations (23)–(27). After choosing a finite element subspace $\mathscr{V}^h \subset \mathscr{V}$ one can just look for weak solutions satisfying the variational problems in a product of this subspace. Here we shall use $\mathscr{V} = H^1(\Omega)$ and the standard piecewise linear elements

$$\mathscr{V}^h = \{v \in C(\Omega) | v|_T \text{ is linear polynomial for } T \in \mathscr{T}\}, \tag{28}$$

where $\mathscr{T}$ is a decomposition of the polygonal domain Ω into triangles or tetrahedra. In the case of periodic boundary conditions on part of the boundary $\Gamma_{\text{per}} \subset \partial\Omega$, the corresponding periodic subspaces of $\mathscr{V}$ and $\mathscr{V}^h$ are used. Moreover we assume natural boundary conditions for all variables on the boundary $\partial\Omega \setminus \Gamma_{\text{per}}$.

The finite element semi-discretization of regularized mean curvature flow consists in finding (ϕ, ω) such that for all t, $\phi(t), \omega(t) \in \mathscr{V}^h$ and $\partial_t\phi(t) \in \mathscr{V}^h$ solve (23), (24).

By analogous reasoning we can restrict the solution (ϕ, μ, ω) of the regularized anisotropic surface diffusion flow to the finite element subspace, and obtain the semi-discrete solution via (25)–(27) for all test functions $\psi, \eta, \vartheta \in \mathscr{V}^h$.

3.2. Semi-implicit time discretization

The appropriate time discretization of the flows is a very challenging problem due to the strongly nonlinear and high-order differential operators. It seems obvious that an explicit time discretization is not a good choice due to severe time step restrictions and in particular due to the instabilities arising from the explicit computation of high-order derivatives. On the other hand, fully implicit time discretizations yield stability, but enforce the solution of strongly nonlinear equations in each time step, which is a difficult task and in any case creates a high computational effort.

Because of the deficiencies of explicit and fully implicit schemes, we try to construct semi-implicit schemes based on the solution of linear problems in each time step. Semi-implicit schemes seem to be the most common approach for the numerical treatment of second and higher order geometric flows based on level set and graph representations (cf. [14–16,18,40]). In all these approaches mentioned before the semi-implicit discretizations have been derived by ad hoc arguments, taking into account some special structure of equations. For more complicated surface energies including curvature terms, it is not obvious how to generalize these approaches. In the case of the Willmore flow (which can be considered as a special case of the regularized anisotropic mean

curvature flow with $\gamma \equiv 0$ and $\epsilon^2 = 1$) Droske and Rumpf [18] found two semi-implicit schemes and their properties still remain rather unclear. Therefore, we shall use a different approach to the time discretization based on the gradient flow formulations. Such an approach has been proposed for this problem in the graph case in [9], and allows to obtain a semi-implicit scheme by second-order approximations of the metric tensor and the energy. For Willmore flow we end up with the same time discretization as the symmetric one in Droske and Rumpf [18].

We start by constructing an approximation to the energy functional, respectively, the Lagrange functional Λ defined in (16). Our aim is to construct a quadratic approximation $\widehat{\Lambda}$ of Λ such that

$$\widehat{E}[\phi] = \sup_{\omega} \widehat{\Lambda}(\phi, \omega) = \sup_{\omega} \Lambda(\phi, \omega) + \mathcal{O}(\tau) = E[\phi] + \mathcal{O}(\tau)$$

and

$$\widehat{E}'[\phi] = E'[\phi] + \mathcal{O}(\tau).$$

In order to obtain such a first-order approximation, we perform a Taylor expansion of the Lagrange functional around the previous time step, i.e. we expand (with the notation $\phi = \phi(t+\tau)$, $\omega = \omega(t+\tau)$, $\phi_0 = \phi(t)$, $\omega_0 = \omega(t)$)

$$\widehat{\Lambda}[\phi, \omega] = \Lambda[\phi_0, \omega_0] + \Lambda'[\phi_0, \omega_0](\phi - \phi_0, \omega - \omega_0) + \frac{1}{2} Q(\phi - \phi_0, \omega - \omega_0),$$

where Q is a quadratic functional used for stabilization purposes. A natural choice for the quadratic functional would be the Hessian of Λ at the previous time step, i.e.

$$Q(\phi - \phi_0, \omega - \omega_0) = \Lambda''[\phi_0, \omega_0](\phi - \phi_0, \omega - \omega_0)^2.$$

The first variations of the functional Λ defined in (16) are given by ($\gamma_z := D\gamma$)

$$\partial_\phi \Lambda[\phi_0, \omega_0]\eta = \int_\Omega \left(\gamma_z(\nabla\phi_0) \cdot \nabla\eta + \frac{\epsilon^2}{2} \frac{\nabla\eta \cdot \nabla\phi_0}{|\nabla\phi_0|^3} \omega_0^2 + \epsilon^2 \frac{(\mathbf{P}_0 \nabla\eta) \cdot \nabla\omega_0}{|\nabla\phi_0|} \right) \mathrm{d}x$$

$$\partial_\omega \Lambda[\phi_0, \omega_0]\vartheta = \int_\Omega \left(-\epsilon^2 \frac{\omega_0 \vartheta}{|\nabla\phi_0|} + \epsilon^2 \frac{\nabla\phi_0 \cdot \nabla\vartheta}{|\nabla\phi_0|} \right) \mathrm{d}x,$$

with $\mathbf{P}_0 = \mathbf{I} - \frac{\nabla\phi_0}{|\nabla\phi_0|} \otimes \frac{\nabla\phi_0}{|\nabla\phi_0|}$, and the second by ($\gamma_{zz} := D^2\gamma$)

$$\partial_{\phi\phi} \Lambda[\phi_0, \omega_0](\eta, \eta) = \int_\Omega (\gamma_{zz}(\nabla\phi_0)\nabla\eta) \cdot \nabla\eta \, \mathrm{d}x + \epsilon^2 R[\phi_0, \omega_0](\eta, \eta) \, \mathrm{d}x$$

$$\partial_{\omega\omega} \Lambda[\phi_0, \omega_0](\vartheta, \vartheta) = -\epsilon^2 \int_\Omega \frac{\vartheta^2}{|\nabla\phi_0|} \mathrm{d}x$$

$$\partial_{\phi\omega} \Lambda[\phi_0, \omega_0](\eta, \vartheta) = \epsilon^2 \int_\Omega \left(\frac{\omega_0 \vartheta \nabla\phi_0 \cdot \nabla\eta}{|\nabla\phi_0|^3} + \frac{\mathbf{P}_0 \nabla\eta \cdot \nabla\vartheta}{|\nabla\phi_0|} \right) \mathrm{d}x.$$

Here R denotes the term arising from the variation of $\int_\Omega \frac{(\mathbf{P}\nabla\eta)\cdot\nabla\omega}{|\nabla\phi|} \, \mathrm{d}x$.

As mentioned before, we need not use the full second derivative as a stabilization functional, but instead use a quadratic functional Q for stabilization purpose. Ideally, such a quadratic functional should be convex with respect to ϕ and concave with respect to ω, since we later want to minimize, respectively, maximize with respect to these variables. Therefore, we use the obviously convex and concave parts in the second variations of Λ for the construction of the quadratic functional. In addition, we add a mixed term involving $\nabla\eta \cdot \nabla\vartheta$ since it corresponds to the highest-order differential operator in the original equation. This motivates a choice of the form

$$Q(\eta, \vartheta) = \int_\Omega \left((\gamma_{zz}(\nabla\phi_0)\nabla\eta) \cdot \nabla\eta + \frac{\epsilon^2}{2} \frac{|\nabla\eta|^2}{|\nabla\phi_0|^3} \omega_0^2 - \epsilon^2 \frac{\vartheta^2}{|\nabla\phi_0|} + 2\epsilon^2 \frac{\nabla\eta \cdot \nabla\vartheta}{|\nabla\phi_0|} \right) \mathrm{d}x.$$

In order to avoid an anisotropy tensor caused by $\gamma_{zz}(\nabla\phi_0)$ we use a similar approach as in [14], and approximate it by $\frac{\lambda}{|\nabla\phi_0|^2}\gamma(\nabla\phi_0)\mathbf{I}$ with λ large enough such that (note the equal scaling of both terms due to the one-homogeneity of γ)

$$\frac{\lambda}{|\nabla\phi_0|^2}\gamma(\nabla\phi_0)\mathbf{I} \geqslant \gamma_{zz}(\nabla\phi_0).$$

This yields the modified quadratic functional

$$\widehat{Q}(\eta,\vartheta) = \int_\Omega \left(\frac{\lambda}{|\nabla\phi_0|^2}\gamma(\nabla\phi_0)|\nabla\eta|^2 + \frac{\epsilon^2}{2}\frac{|\nabla\eta|^2}{|\nabla\phi_0|^3}\omega_0^2 - \epsilon^2\frac{\vartheta^2}{|\nabla\phi_0|} + 2\epsilon^2\frac{\nabla\eta\cdot\nabla\vartheta}{|\nabla\phi_0|}\right)\mathrm{d}x.$$

Motivated by the above discussion we consider the following quadratic approximation to the Lagrange functional (which is consistent to first-order)

$$\begin{aligned}\widehat{\Lambda}[\phi,\omega] &= \Lambda[\phi_0,\omega_0] + \Lambda'[\phi_0,\omega_0](\phi-\phi_0,\omega-\omega_0) + \frac{1}{2}\widehat{Q}(\phi-\phi_0,\omega-\omega_0)\\ &= \int_\Omega \left(\gamma(\nabla\phi_0) + \gamma_z(\nabla\phi_0)\cdot(\nabla\phi-\nabla\phi_0) + \lambda\gamma(\nabla\phi_0)\frac{(\nabla\phi-\nabla\phi_0)^2}{2|\nabla\phi_0|^2}\right)\mathrm{d}x\\ &\quad + \epsilon^2\int_\Omega\left(-\frac{\omega^2}{2|\nabla\phi_0|} + \frac{|\nabla\phi|^2-|\nabla\phi_0|^2}{4|\nabla\phi_0|^3}\omega_0^2\right)\mathrm{d}x\\ &\quad + \epsilon^2\int_\Omega\left(\frac{\nabla\phi\cdot\nabla\omega}{|\nabla\phi_0|} - \frac{[(\nabla\phi-\nabla\phi_0)\cdot\nabla\phi_0][\nabla\phi_0\cdot\nabla\omega_0]}{|\nabla\phi_0|^3}\right)\mathrm{d}x.\end{aligned}$$

For both flows, a time step of size τ from $\phi_0 := \phi(t)$ to $\phi = \phi(t+\tau)$ is specified by the solution of the variational problem

$$\inf_{\phi\in\mathscr{V}^h}\sup_{\omega\in\mathscr{V}^h}\left(\frac{1}{2\tau}g_{\phi_0}(\phi-\phi_0,\phi-\phi_0) + \widehat{\Lambda}[\phi,\omega]\right).$$

The variations with respect to ϕ and ω then yield the fully discrete system for the time step

$$\frac{1}{\tau}g_{\phi_0}(\phi-\phi_0,\eta) + \partial_\phi\widehat{\Lambda}[\phi,\omega]\eta = 0 \quad \forall\eta\in\mathscr{V}^h \tag{29}$$

$$\partial_\omega\widehat{\Lambda}[\phi,\omega]\vartheta = 0 \qquad \forall\vartheta\in\mathscr{V}^h. \tag{30}$$

The specific statements of the fully discrete schemes for both anisotropic flows will be given in the following section.

3.3. Fully discrete schemes

We now provide the detailed forms of the fully discrete schemes derived above by quadratic approximations of metric and energy. The time grid for the computation is given by $0 = t_0 < t_1 < \ldots t_n = T$, with $\tau_k := t_{k+1} - t_k$ denoting the local time step. The discrete solution at time step t_k will be denoted by $\phi^k := \phi(t_k) \in \mathscr{V}^h$ and $\omega^k := \omega(t_k) \in \mathscr{V}^h$, respectively.

For the regularized anisotropic mean curvature flow, we can insert the form of g_ϕ given in (20) directly into (29) and obtain the discrete formulation as computing $\phi^{k+1}, \omega^{k+1} \in \mathscr{V}^h$ satisfying

$$\int_\Omega \beta \frac{(\phi^{k+1}-\phi^k)\eta}{\tau_k|\nabla\phi^k|}\,\mathrm{d}x + \int_\Omega \frac{\epsilon^2}{2}\frac{\nabla\phi^{k+1}\cdot\nabla\eta}{|\nabla\phi^k|^3}(\omega^k)^2\,\mathrm{d}x + \int_\Omega \left(\gamma_z(\nabla\phi^k)\cdot\nabla\eta + \frac{\lambda}{|\nabla\phi_k|^2}\gamma(\nabla\phi^k)\nabla\eta\cdot(\nabla\phi^{k+1}-\nabla\phi^k)\right)\mathrm{d}x + \int_\Omega \left(\epsilon^2\frac{\nabla\eta\cdot\nabla\omega^{k+1}}{|\nabla\phi^k|} - \epsilon^2\frac{[\nabla\eta\cdot\nabla\phi^k][\nabla\omega^k\cdot\nabla\phi^k]}{|\nabla\phi^k|^3}\right)\mathrm{d}x = 0 \tag{31}$$

$$\int_\Omega \frac{\omega^{k+1}\vartheta}{|\nabla\phi^k|}\mathrm{d}x - \int_\Omega \frac{\nabla\phi^{k+1}\cdot\nabla\vartheta}{|\nabla\phi^k|}\mathrm{d}x = 0 \tag{32}$$

for all $\eta,\vartheta\in\mathscr{V}^h$.

In the case of regularized anisotropic surface diffusion using (21) and (29) leads to the following fully-discrete scheme for curvature regularized anisotropic surface diffusion: Each time step consists in finding $\phi^{k+1},\mu^{k+1},\omega^{k+1}\in\mathscr{V}^h$ such that

$$\int_\Omega \frac{(\phi^{k+1}-\phi^k)\psi}{\tau_k}\,\mathrm{d}x - \int_\Omega v(\mathbf{P}^k\nabla\mu^{k+1})\cdot\nabla\psi|\nabla\phi^k|\,\mathrm{d}x = 0 \tag{33}$$

$$\int_\Omega \mu^{k+1}\eta\,\mathrm{d}x + \int_\Omega \frac{\epsilon^2}{2}\frac{\nabla\phi^{k+1}\cdot\nabla\eta}{|\nabla\phi^k|^3}(\omega^k)^2\,\mathrm{d}x + \int_\Omega \left(\gamma_z(\nabla\phi^k)\cdot\nabla\eta + \frac{\lambda}{|\nabla\phi_k|^2}\gamma(\nabla\phi^k)\nabla\eta\cdot(\nabla\phi^{k+1}-\nabla\phi^k)\right)\mathrm{d}x + \int_\Omega \left(\epsilon^2\frac{\nabla\eta\cdot\nabla\omega^{k+1}}{|\nabla\phi^k|} - \epsilon^2\frac{[\nabla\eta\cdot\nabla\phi^k][\nabla\omega^k\cdot\nabla\phi^k]}{|\nabla\phi^k|^3}\right)\mathrm{d}x = 0 \tag{34}$$

$$\int_\Omega \frac{\omega^{k+1}\vartheta}{|\nabla\phi^k|}\mathrm{d}x - \int_\Omega \frac{\nabla\phi^{k+1}\cdot\nabla\vartheta}{|\nabla\phi^k|}\mathrm{d}x = 0 \tag{35}$$

for all $\eta,\vartheta,\psi\in\mathscr{V}^h$.

3.4. Stability

With the above derivation of the time discretization one obtains a straigh-forward possibility to check stability of the scheme, in particular in terms of the energy dissipation. We shall discuss the general approach in the following and remark on the application to the specific energies we are dealing with, but do not provide the tedious detailed calculations.

In order to obtain stability we would like to derive an inequality of the form

$$\frac{c}{2\tau}g_{\phi(t)}(\phi(t+\tau)-\phi(t),\phi(t+\tau)-\phi(t)) + E[\phi(t+\tau)] \leqslant E[\phi(t)] \tag{36}$$

for some constant $c>0$, which would yield energy dissipation as well as the boundedness of the discrete time derivative and, as a direct consequence, stability of the scheme. As we shall see, this goal can be achieved by a Lagrange functional $\widehat{\Lambda}$ satisfying the following two properties (we use the same notation ϕ_0 for the previous time step as in the above sections):

- *Minorization at previous time step*:

$$\sup_\omega \widehat{\Lambda}(\phi_0,\omega) \leqslant \sup_\omega \Lambda(\phi_0,\omega). \tag{37}$$

- *Majorization with dissipation*: For all $\psi\in\mathscr{V}^h$ and some constant $c\in(0,1)$

$$\sup_\omega \left(\widehat{\Lambda}(\psi,\omega) + \frac{1-c}{2\tau}g_{\phi_0}(\psi-\phi_0,\psi-\phi_0)\right) \geqslant \sup_\omega \Lambda(\psi,\omega). \tag{38}$$

If (37) and (38) are satisfied, then we have

$$\begin{aligned}\frac{c}{2\tau}g_{\phi_0}(\phi-\phi_0,\phi-\phi_0)+E[\phi] &= \frac{c}{2\tau}g_{\phi_0}(\phi-\phi_0,\phi-\phi_0)+\sup_\omega \Lambda(\phi,\Omega)\\ &\leqslant \frac{1}{2\tau}g_{\phi_0}(\phi-\phi_0,\phi-\phi_0)+\sup_\omega \widehat{\Lambda}(\phi,\Omega)\leqslant \sup_\omega \widehat{\Lambda}(\phi_0,\Omega)\leqslant \sup_\omega \Lambda(\phi_0,\Omega)\\ &= E[\phi_0]\end{aligned}$$

and hence, (36) holds.

With our construction of $\widehat{\Lambda}$, (37) becomes

$$\sup_\omega\left(\Lambda[\phi_0,\omega_0]+\Lambda'[\phi_0,\omega_0](0,\omega-\omega_0)+\frac{1}{2}Q(0,\omega-\omega_0)\right)\leqslant \sup_\omega \Lambda[\phi_0,\omega_0],$$

which can indeed be achieved in our case with the quadratic functional Q being concave in the second variable. The inequality (38) can at least be obtained for sufficiently small time step τ, since the metric term will then dominate. As a consequence, a conditional stability is obtained, which is on the other hand not too surprising for a semi-implicit time discretization of a problem with nonconvex energy. In the case of anisotropic mean curvature flow it turns out that a condition of the form $\tau\sim h_{\text{grid}}^2$ is sufficient, whereas for surface diffusion one obtains $\tau\sim h_{\text{grid}}^4$, with h_{grid} the spatial grid size. At a first glance such stability bounds appear to be strong, but on the other hand we need such small time steps in the level set approach anyway as described below. In practice, one can always obtain stability by adjusting the time step so that (36) is satisfied, which might also allow to proceed to larger time steps.

4. Implementation

The derived numerical schemes are implemented in the adaptive finite element toolbox AMDiS [4]. The toolbox provides a framework for the efficient solution of systems of partial differential equations by adaptive finite elements. For details on the software we refer to [46,43,47]. Here we only describe the resulting linear systems for the two problems of curvature regularized anisotropic mean curvature flow and curvature regularized anisotropic surface diffusion.

4.1. Discrete formulation

Introducing the weighted mass and stiffness matrices

$$M[f]:=\left(\int_\Omega f\varphi_i\varphi_j\,\mathrm{d}x\right)_{i,j},$$

$$L[f]:=\left(\int_\Omega f\nabla\varphi_i\nabla\varphi_j\,\mathrm{d}x\right)_{i,j},\quad L[A]:=\left(\int_\Omega A\nabla\varphi_i\nabla\varphi_j\,\mathrm{d}x\right)_{i,j}$$

with functions $f:\Omega\to\mathbb{R}$ and $A:\Omega\to\mathbb{R}^{d\times d}$, and basis functions $\varphi_i\in\mathscr{V}^h$, the matrices and right-hand side vectors in the discrete representation of the two problems are

$$\begin{aligned}M_1&:=M[|\nabla\phi^k|_\delta^{-1}], & M_2&:=M[1],\\ M_3&:=M[\beta|\nabla\phi^k|_\delta^{-1}], & L_1&:=L[(W^k)^2|\nabla\phi^k|_\delta^{-3}],\\ L_3&:=L[|\nabla\phi^k|_\delta^{-1}], & L_4&:=L[(id-P[\phi^k])|\nabla\phi^k|_\delta^{-1}],\\ L_5&:=L\left[\gamma\left(\frac{\nabla\phi^k}{|\nabla\phi^k|_\delta}\right)|\nabla\phi^k|_\delta^{-1}\right], & L_6&:=L[\nu P[\phi^k]|\nabla\phi^k|_\delta],\\ G&:=\left(\int_\Omega \gamma_z\left(\frac{\nabla\phi^k}{|\nabla\phi^k|_\delta}\right)\nabla\varphi_j\,\mathrm{d}x\right)_j.\end{aligned}$$

As the norm $|\nabla\phi^k|$ may become small away from the interface (signed distance property is only maintained near the interface, see Section 5), we use the regularization $|\nabla\phi^k|_\delta = (\delta^2 + |\nabla\phi^k|^2)^{1/2}$, with $0 < \delta \ll 1$. Note that this would also be necessary when topological changes occur. The operator $P[\phi]$ is defined through $P[\phi] = I - \frac{\nabla\phi}{|\nabla\phi|_\delta} \otimes \frac{\nabla\phi}{|\nabla\phi|_\delta}$ which for $\delta = 0$ is the projection to the tangential spaces of the level sets of ϕ. With these notions the linear systems are as follows.

4.2. Linear system for curvature regularized anisotropic mean curvature flow

We expand ϕ^{k+1} and ω^{k+1} as

$$\phi^{k+1} = \sum_{i=1}^{L} \Phi_i^{k+1}\varphi_i, \quad \omega^{k+1} = \sum_{i=1}^{L} W_i^{k+1}\varphi_i,$$

where L is the dimension of $\mathscr{V}^h$. The linear system for the coefficient vectors obtained from (31), (32) reads

$$\begin{pmatrix} M_3 + \tau\frac{\epsilon^2}{2}L_1 + \tau\lambda L_5 & \tau\epsilon^2 L_3 \\ -L_3 & M_1 \end{pmatrix} \begin{pmatrix} \Phi^{k+1} \\ W^{k+1} \end{pmatrix} = \begin{pmatrix} M_3\Phi^k + \tau\lambda L_5\Phi^k + \tau\epsilon^2 L_4 W^k - \tau G \\ 0 \end{pmatrix}.$$

Using a Schur complement approach, we arrive at the following linear equation for the unknown Φ^{k+1}:

$$\left(M_3 + \tau\frac{\epsilon^2}{2}L_1 + \tau\lambda L_5 + \tau\epsilon^2 L_3 M_1^{-1} L_3\right)\Phi^{k+1} = M_3\Phi^k + \tau\lambda L_5\Phi^k + \tau\epsilon^2 L_4 W^k - \tau G$$

with $W^k = M_1^{-1}L_3\Phi^k$. Since the system matrix is symmetric positive definite a CG-solver is used for the linear systems arising in each times step. The inverse mass matrix M_1^{-1} is calculated explicitly using mass lumping.

4.3. Linear system for curvature regularized anisotropic surface diffusion

We expand ϕ^{k+1}, μ^{k+1} and ω^{k+1} as

$$\phi^{k+1} = \sum_{i=1}^{L} \Phi_i^{k+1}\varphi_i, \quad \mu^{k+1} = \sum_{i=1}^{L} U_i^{k+1}\varphi_i \quad \omega^{k+1} = \sum_{i=1}^{L} W_i^{k+1}\varphi_i.$$

The linear system obtained from eqs. (33)–(35) then reads

$$\begin{pmatrix} M_2 & -\tau L_6 & 0 \\ \frac{\epsilon^2}{2}L_1 + \lambda L_5 & M_2 & \epsilon^2 L_3 \\ -L_3 & 0 & M_1 \end{pmatrix} \begin{pmatrix} \Phi^{k+1} \\ U^{k+1} \\ W^{k+1} \end{pmatrix} = \begin{pmatrix} M_2\Phi^k \\ \lambda L_5\Phi^k + \epsilon^2 L_4 W^k - G \\ 0 \end{pmatrix}.$$

Again, a Schur complement approach leads to a linear system for the unknown Φ^{k+1}:

$$\left[M_2 + \tau L_6 M_2^{-1}\left(\frac{\epsilon^2}{2}L_1 + \lambda L_5 + \epsilon^2 L_3 M_1^{-1} L_3\right)\right]\Phi^{k+1} = M_2\Phi^k + \tau L_6 M_2^{-1}(\lambda L_5\Phi^k + \epsilon^2 L_4 W^k - G)$$

with $W^k = M_1^{-1}L_3\Phi^k$. The Schur complement system is then solved with the Krylov-subspace method GMRES. Again, the inverse mass matrices M_1^{-1} and M_2^{-1} are calculated with mass lumping.

5. Numerical results

We test the described numerical algorithm on several two- and three-dimensional problems for curvature regularized anisotropic mean curvature flow (reg. MCF) and curvature regularized anisotropic surface diffusion (reg. SD). In the case of closed curves or surfaces natural boundary conditions are used. In all other examples, which deal with the evolution of a thin film, periodic boundary conditions on the side walls and natural boundary conditions at the top and bottom are imposed.

Throughout the simulations we use the regularized anisotropy

$$\hat{\gamma} = \gamma + \epsilon^2 \frac{1}{2} h^2, \quad \gamma(p) = |p| + a \sum_{k=1}^{d} \frac{p_k^4}{|p|}, \quad d = 2, 3,$$

with h being the mean curvature and p_k denoting the k-th spatial component of $p \in \mathbb{R}^d$. If not stated otherwise, we choose $a = 1.0$ (i.e. γ is non-convex) and $\epsilon = 0.1$. Furthermore, in order to concentrate on the anisotropy in the surface free energy, we chose $\beta = v = 1$.

The computational grid is adaptively refined at the zero level set, to provide a high resolution at interface regions without increasing the computational cost away from the interface. Adaptive refinement and coarsening is done by bisectioning. Fig. 1 shows an example of a two-dimensional grid. In the numerical examples, h_{grid} denotes the grid size at the zero level set. Furthermore, we reinitialize the level set function from time to time to ensure an approximate signed-distance property. The reinitialization algorithm is based on a local Hopf-Lax formula for the solution of the eikonal equation. We use the explicit formula given by [8] in two dimensions and [43] in three dimensions. If not stated otherwise, a reinitialization step is performed whenever the gradient of the level set function does not fulfill $0.5 \leqslant |\nabla \phi| \leqslant 2.0$ at the zero level set.

As already pointed out in the introduction, a non-convex anisotropy function γ will lead to the formation of facets in the evolving interface. The final facet angle for non-closed interfaces is determined by the Wulff angles, i.e. the boundaries of the range of missing orientations of the Wulff shape. An example of the Wulff shape $\mathscr{W}_\gamma$ for a non-convex anisotropy is depicted in Fig. 2. The Wulff angles may be calculated by determining the intersection points.

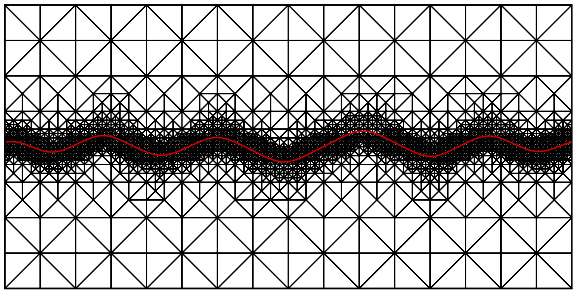

Fig. 1. Grid adaptively refined at zero level set.

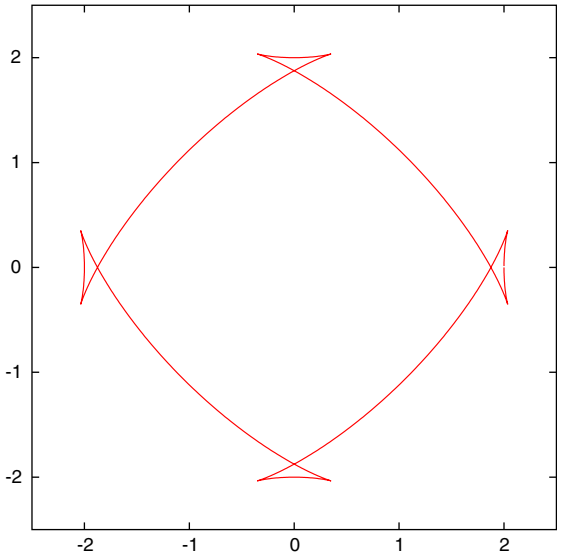

Fig. 2. The Wulff shape is obtained by omitting the swallow tails ("missing orientations") of the parameterized curve $S^1 \ni z \mapsto D\gamma(z)$ for anisotropy γ with $a = 1.0$.

Before presenting our numerical results, we comment on the choice of parameters in the simulations. First the spatial grid size h_{grid} is connected to the regularization parameter ϵ as $h_{\text{grid}} \sim \epsilon$ since ϵ is the length scale on which the rounding of the corners in the Wulff shape happens. Moreover the parameter δ regularizing the norm of the gradient of ϕ is chosen as $\delta \approx h_{\text{grid}}$. The time step τ is chosen as

$$\tau \sim \frac{h_{\text{grid}}^4}{\epsilon^2} \sim h_{\text{grid}}^2 \quad \text{mean curvature}$$

$$\tau \sim \frac{h_{\text{grid}}^6}{\epsilon^2} \sim h_{\text{grid}}^4 \quad \text{surface diffusion.}$$

The parameter λ does depend on the strength of the anisotropy γ, it is chosen to achieve the majorization property discussed in Section 3.4. In all our examples we have chosen $\lambda = 1.0$.

5.1. Regularized mean curvature flow

5.1.1. Circle

We start with a closed curve and demonstrate the evolution of a circle towards the Wulff shape. Fig. 3 shows the evolution of a circle towards the Wulff shape. For the unstable orientations at $\theta = 0, \pi/2, \pi, 3\pi/2$ oscillations can be observed, which lead to a local hill-valley struture, which subsequently coarsens and forms the final rounded corner. The shape at $t = 0.035$ is not a steady state. The evolution law is not area conserving and the curve continues to shrink in time. However, the shape does not change after $t = 0.035$.

5.1.2. Sphere

As a second example, we have a look at the three-dimensional counterpart, a sphere, and its development towards the Wulff shape. Fig. 4 first shows the evolution of the sphere towards the Wulff shape and then the shrinking of the closed surface.

5.1.3. Omega shape

Next, we deal with an interface, whose shape is not a graph at $t = 0$. Fig. 5 shows the evolution at several time instants. Oscillations can be observed on the flat parts with orientation $\theta = 0$. The remaining parts

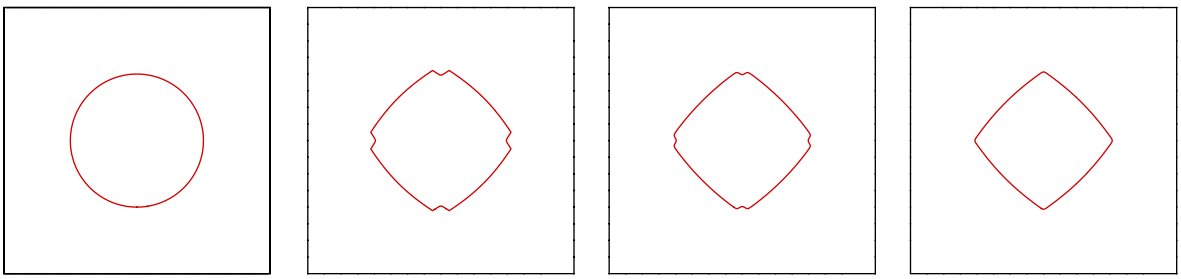

Fig. 3. Evolution of closed curve to Wulff shape under reg. MCF. $[0,4] \times [0,4]$-grid, $h_{\text{grid}} = 0.015625$, $a = 3.0$, $\epsilon = 0.05$, $\tau = 10^{-5}$. From left to right: zero level set at time $t = 0.0$, 0.01, 0.025, 0.035.

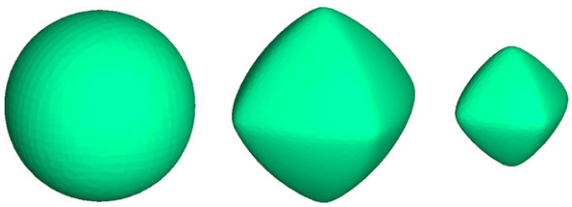

Fig. 4. Evolution of closed surface to Wulff shape under reg. MCF. $[0,4] \times [0,4] \times [0,4]$-grid, $h_{\text{grid}} = 0.0625$, $\tau = 10^{-4}$, reinitialization every 50th time step. From left to right: zero level set at time $t = 0.0$, 0.04, 0.16.

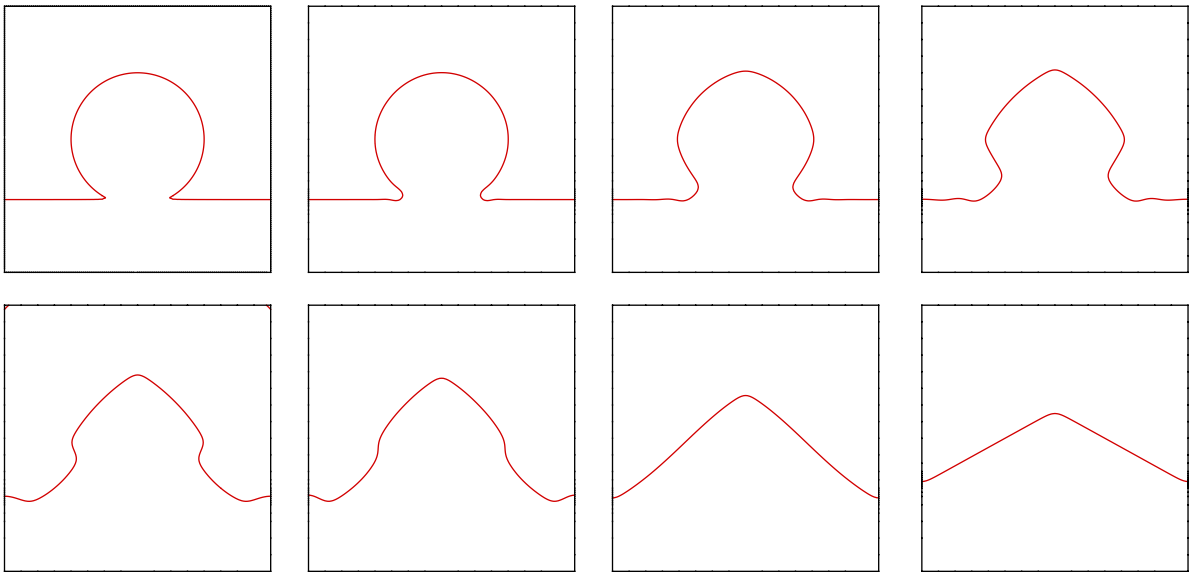

Fig. 5. Faceting of zero level set under reg. MCF. $[0,4] \times [0,4]$-grid, $h_{\text{grid}} = 0.03125$, $\tau = 10^{-5}$, reinitialization every 10th time step. From top left to bottom right: zero level set at time $t = 0.0$, 0.001, 0.01, 0.03, 0.08, 0.1, 0.2, 1.0.

develop towards a shape with rounded corners connected by nearly straight segments (“facets”) (top row of Fig. 5). Due to the periodic boundary conditions, this is not the energy minimizing shape. The surface energy can further be reduced by decreasing the number of rounded corners and the overall curve length, which leads to the final steady state (bottom row of Fig. 5). The numerically measured facet angle at $t = 1.0$ is 26.6°, while the predicted facet angle is 28.8°.

5.1.4. Hill-valley structure in two dimensions

We now deal with a setting, which is close to the described application of thermal annealing and the formation of a hill-valley structure. For these simulations it is useful to consider a linear stability analysis for the orientation $\theta = 0$, see e.g. [17]. Provided the stiffness $\tilde{\gamma}(0) = \gamma(0) + \gamma''(0)$ is negative, the orientation $\theta = 0$ is unstable with most unstable wavelength $\lambda_{\max}$ given by

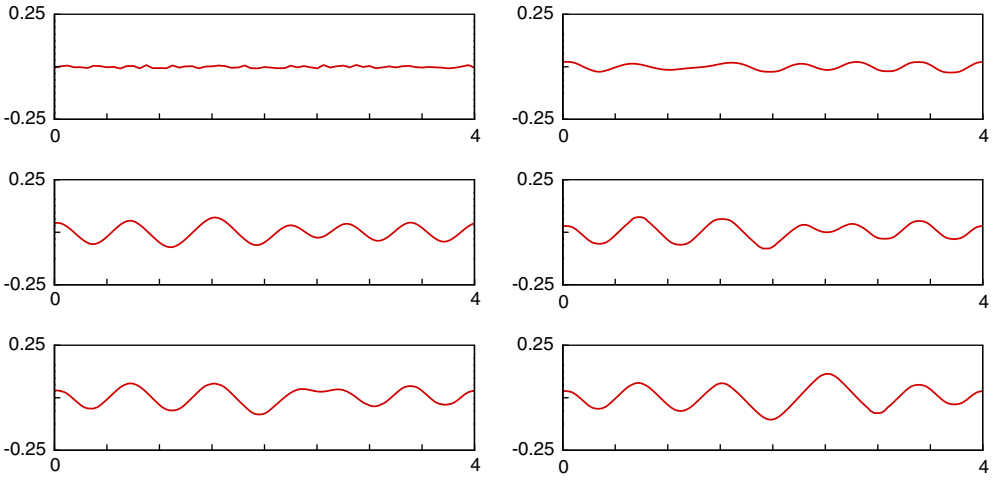

Fig. 6. Faceting and coarsening of zero level set under reg. MCF. $[0,4] \times [0,2]$-grid, $h_{\text{grid}} = 0.03125$, $\tau = 10^{-6}$. From top left to bottom right: zero level set at time $t = 0.0$, 0.035, 0.09, 0.16, 0.2, 0.3.

$$\lambda_{\max} = \frac{2\pi\sqrt{2}\epsilon}{\sqrt{|\tilde{\gamma}(0)|}} \quad \text{with } |\tilde{\gamma}(0)| = |1 - 3a|.$$

Perturbed straight line. Choosing $\epsilon = 0.1$, $a = 1.0$ yields $\lambda_{\max} \approx 0.63$. As depicted in Fig. 6, a randomly perturbed horizontal line ($\theta = 0$) develops a hill-valley pattern with wavelength $\lambda = 4/6 \approx \lambda_{\max}$. After this initial stage, faceting and subsequent coarsening takes place. The numerically obtained facet angle at $t = 0.3$ is 26.1°, measured at the highest kink, which is close to the predicted facet angle (28.2°).
Superposed sine. The initial curve is a superposition of sine functions. Fig. 7 shows its evolution. The numerically measured facet angle of the final shape at $t = 0.9$ is 23.4° and agrees very well with the predicted facet angle of 24.1°.

5.1.5. Hill-valley structure in three dimensions

We now turn to a three-dimensional setting and simulate the spinodal decomposition of a randomly perturbed initially flat surface into a hill-valley structure and its subsequent coarsening. Fig. 8 shows the evolution of the zero level set at various times. At a first stage a hill-valley structure emerges (spinodal decomposition). After the formation of facets and rounded corners and edges, coarsening starts to take place. A more detailed investigation of the coarsening dynamics will be subject of future research.

5.2. Regularized surface diffusion

5.2.1. Circle

We again start with a closed curve. Fig. 9 shows the evolution of a circle towards the Wulff shape. The area is conserved. In contrast to the curvature regularized anisotropic mean curvature flow problem, oscillations do not occur for the chosen parameter, since the most unstable wavelength is too large.

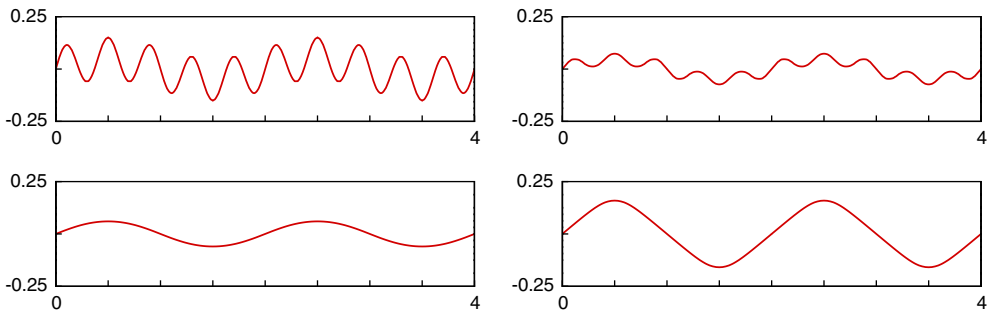

Fig. 7. Faceting of zero level set under reg. MCF. $[0,4] \times [0,2]$-grid, $h_{\text{grid}} = 0.03125$, $a = \frac{2}{3}$, $\tau = 10^{-6}$. From top left to bottom right: zero level set at time $t = 0.0$, 0.003, 0.05, 0.9.

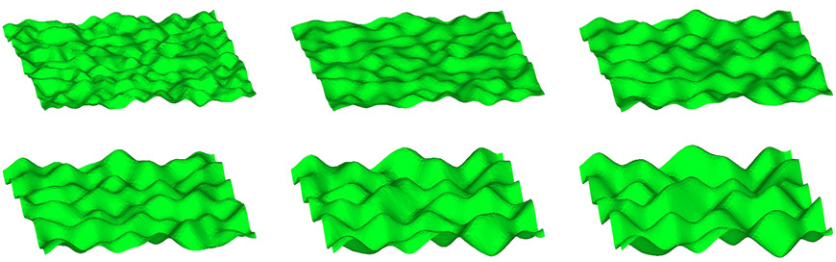

Fig. 8. Faceting and coarsening of zero level set under reg. MCF. $[0,4] \times [0,4] \times [0,1]$-grid, $h_{\text{grid}} = 0.0625$, $\tau = 10^{-5}$. From top left to bottom right: zero level set at time $t = 0.001$, 0.004, 0.02, 0.04, 0.08, 0.12.

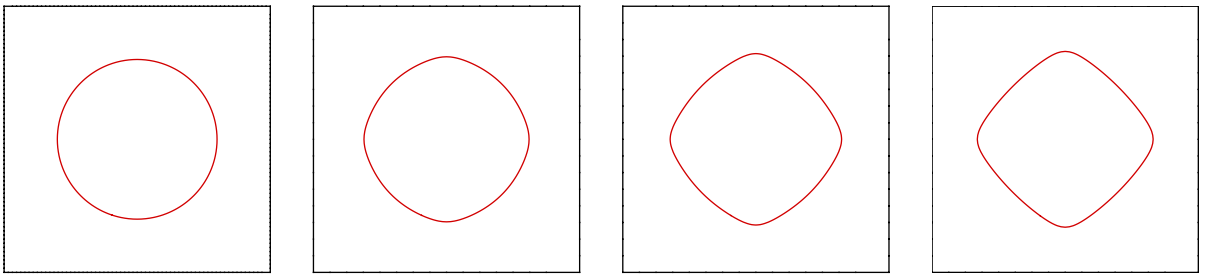

Fig. 9. Evolution of closed curve to Wulff shape under reg. SD. $[0,4] \times [0,4]$-grid, $h_{\text{grid}} = 0.0625$, $\tau = 10^{-6}$, $\epsilon = 0.2$, reinitialization every 50th time step. From left to right: zero level set at time $t = 0.0$, 0.001, 0.003, 0.01.

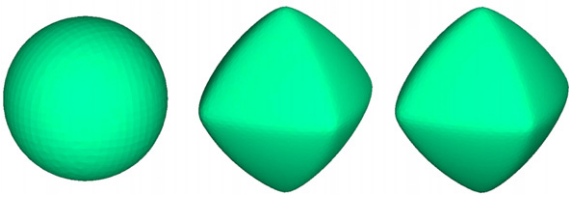

Fig. 10. Evolution of closed surface to Wulff shape under reg. SD. $[0,4] \times [0,4] \times [0,4]$-grid, $h_{\text{grid}} = 0.0625$, $\tau = 10^{-6}$, reinitialization every 50th timestep. From left to right: zero level set at time $t = 0.0$, 0.001, 0.007.

5.2.2. Sphere

The evolution of the sphere to the Wulff shape is depicted in Fig. 10. In difference to curvature regularized anisotropic mean curvature flow, we see here the volume conserving behavior.

5.2.3. Omega shape

Fig. 11 shows the evolution at various time steps. The oscillations on the flat parts are much more pronounced than in the case of curvature regularized anistropic mean curvature flow. As expected for the higher

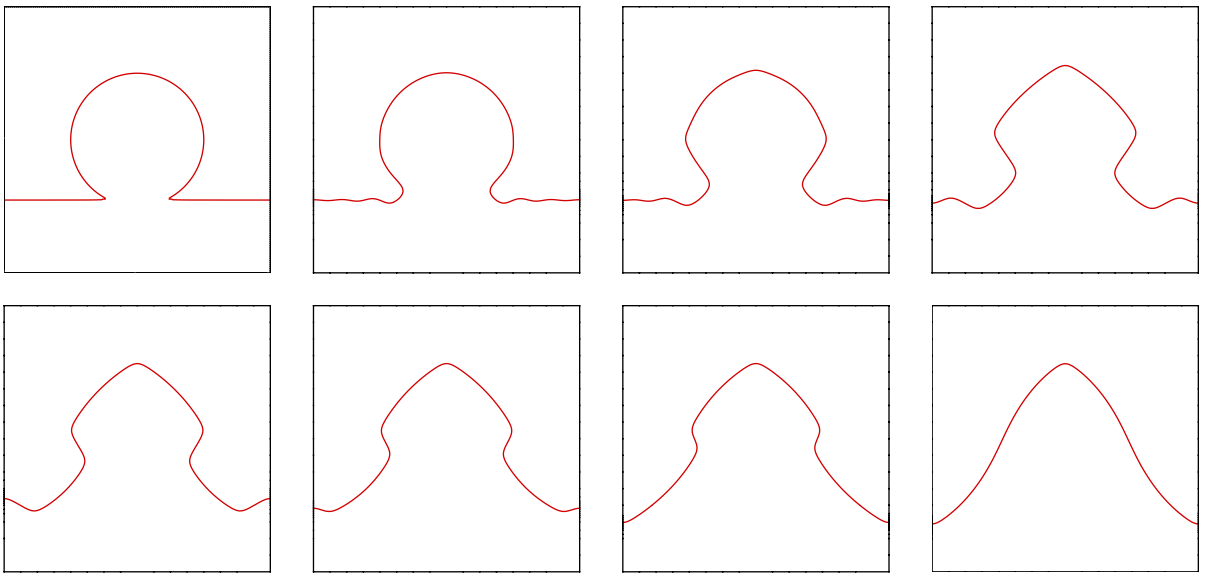

Fig. 11. Faceting of zero level set under reg. SD. $[0,4] \times [0,4]$-grid, $h_{\text{grid}} = 0.03125$, $\tau = 5 \times 10^{-8}$, reinitialization every 100th timestep. From top left to bottom right: zero level set at time $t = 0.0$, 0.0001, 0.0005, 0.003, 0.01, 0.02, 0.03, 0.058.

order equation the time scale at which these ocillations occur and form a local hill-valley structure is much smaller than in Section 5.1.3. However, the formation of the predicted facet angle of the final steady state needs much more time as compared to curvature regularized anisotropic mean curvature flow.

5.2.4. Hill-valley structure in two dimensions

Again we first compute the most unstable wavelength $\lambda_{\max}$ from a linear stability analysis for $\theta = 0$.

$$\lambda_{\max} = 2\pi\epsilon\sqrt{\frac{3}{2|\tilde{\gamma}(0)|}} \quad \text{with} \quad |\tilde{\gamma}(0)| = |1 - 3a|.$$

Perturbed straight line. Choosing $\epsilon = 0.1$, $a = 1.0$ yields $\lambda_{\max} \approx 0.544$. As for the regularized mean curvature flow we observe the spinodal decomposition of a randomly perturbed horizontal line into a hill-valley pattern with wavelength $\lambda = 4/7 \approx \lambda_{\max}$ and subsequent faceting and coarsening, see Fig. 12.
Superposed sine. Fig. 13 shows the evolution of a superposition of sine functions. The damping of the high frequencies is much faster if compared with curvature regularized anisotropic mean curvature flow.

5.2.5. Hill-valley structure in three dimensions

We now turn to a three-dimensional setting and simulate the spinodal decomposition of a randomly perturbed initially flat surface into a hill-valley structure and its subsequent coarsening. Fig. 14 shows the evolution of the zero level set at various times. The formation of facets and the rounded corners and edges can clearly be observed. After the evolution of the right facet angles, coarsening starts. Again this is qualitatively

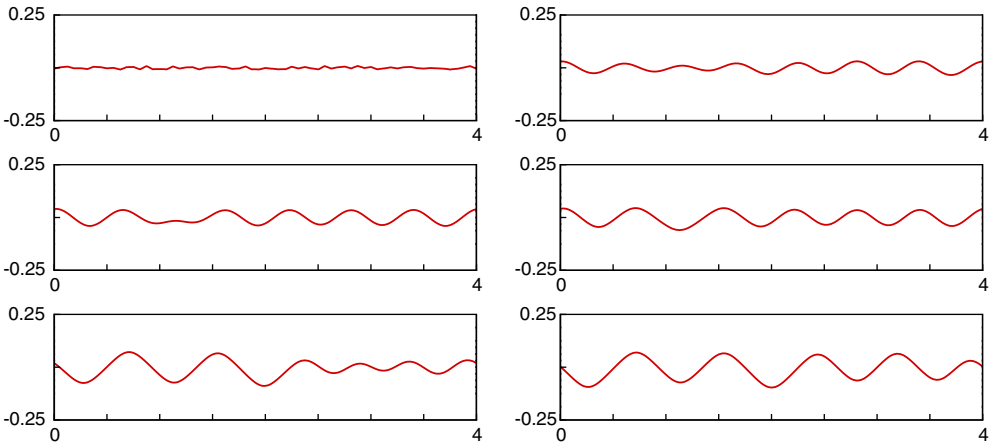

Fig. 12. Faceting and coarsening of zero level set under reg. SD. $[0,4] \times [0,2]$-grid, $h_{\text{grid}} = 0.03125$, $\tau = 10^{-7}$, reinitialization every 50th time step. From top left to bottom right: zero level set at time $t = 0.0$, 0.0004, 0.0017, 0.002, 0.016, 0.018.

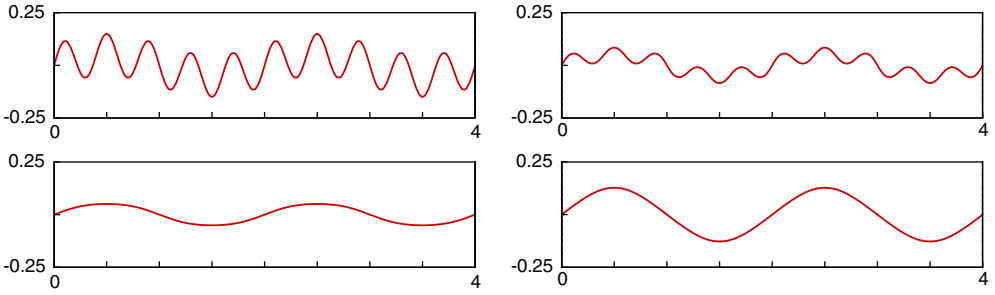

Fig. 13. Faceting of zero level set under reg. SD. $[0,4] \times [0,2]$-grid, $h_{\text{grid}} = 0.03125$, $a = \frac{2}{3}$, $\epsilon = 0.2$, $\tau = 10^{-8}$ until $t = 10^{-5}$, $\tau = 10^{-7}$ until $t = 2 \times 10^{-5}$, then $\tau = 10^{-6}$, reinitialization every 50th timestep. From top left to bottom right: zero level set at time $t = 0.0$, 5×10^{-6}, 2×10^{-5}, 0.081.

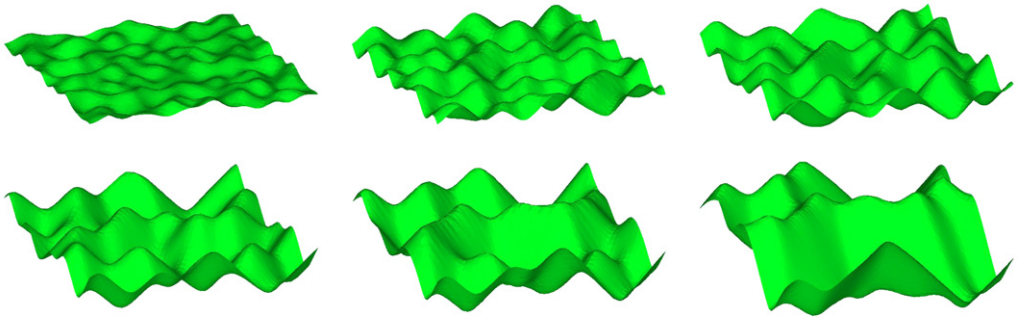

Fig. 14. Faceting and coarsening of zero level set under reg. SD. $[0,4]\times[0,4]\times[0,1]$-grid, $h_{\text{grid}} = 0.0625$, $\tau = 5\times 10^{-6}$. From top left to bottom right: zero level set at time $t = 0.0001$, 0.002, 0.006, 0.012, 0.016, 0.035.

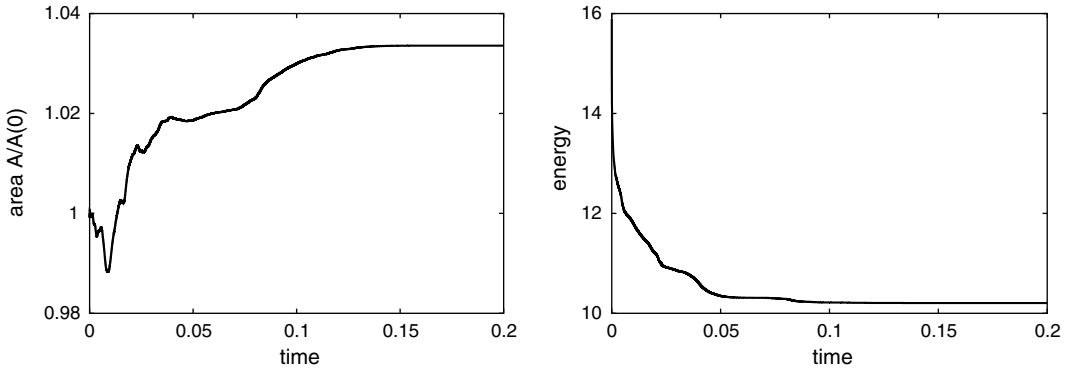

Fig. 15. Area conservation (left) and energy decrease (right) for regularized surface diffusion in example *Omega shape*, see Fig. 11.

similar to the case of curvature regularized anisotropic mean curvature flow but happens on a smaller time scale. A detailed study of the coarsening dynamics and a quantitative comparison of the two different mass transport mechanisms will be subject of future research.

5.2.6. Volume/area conservation and energy decrease

We recall two fundamental properties of motion by curvature regularized anisotropic surface diffusion: It is volume preserving which follows from

$$\begin{aligned}\frac{\mathrm{d}}{\mathrm{d}t}\mathrm{Volume}(t) &= \int_{\Sigma(t)} v(t)\,\mathrm{d}\sigma = \int_{\Sigma(t)} \nabla_\sigma\cdot\left(v\nabla_\sigma\left(h_\gamma - \epsilon\left(\Delta_\sigma h + h\left(\|S\|^2 - \frac{1}{2}h^2\right)\right)\right)\right)\mathrm{d}\sigma\\ &= -\int_{\Sigma(t)} v\nabla_\sigma\left(h_\gamma - \epsilon\left(\Delta_\sigma h + h\left(\|S\|^2 - \frac{1}{2}h^2\right)\right)\right)\cdot\nabla_\sigma 1\,\mathrm{d}\sigma = 0\end{aligned}$$

and energy decreasing, which follows from the construction as the H^{-1}-gradient flow.

Fig. 15 shows the two properties for the computation in Section 5.2.3. The volume is preserved within a tolerance of 4%.

Acknowledgments

The work of M.B. has been supported by the Austrian National Science Foundation FWF through project SFB F 013/08 and the Johann Radon Institute for Computational and Applied Mathematics (Austrian Academy of Sciences). A.V. and C.S. have been supported by the German Science Foundation DFG through project SFB 611/B3. M.B. and A.V. acknowledge partial support by the NSF-funded Institute for Pure and

Applied Mathematics (IPAM), UCLA, part of this work has been performed during their participation in the IPAM program *Bridging Time and Length Scales in Materials Science and Bio-Physics*.

References

[1] F. Almgren, J.E. Taylor, Optimal geometry in equilibrium and growth, Fractals 3 (1996) 713–723.
[2] L. Ambrosio, N. Gigli, G. Savare, Metric Gradient Flows, Birkhäuser, Basel, 2005.
[3] L. Ambrosio, N. Fusco, D. Pallara, Functions of bounded variation and free discontinuity problems, Oxford University Press, Oxford, 2000.
[4] <www.caesar.de/amdis.html>.
[5] M. Bertalmio, L.T. Cheng, S. Osher, G. Sapiro, Variational problems and partial differential equations on implicit surfaces: the framework and examples in image processing and pattern formation, J. Comput. Phys. 174 (2001) 759–780.
[6] M. Bertalmio, F. Memoli, L.T. Cheng, G. Sapiro, S. Osher, Variational problems and partial differential equations on implicit surfaces: bye triangulated surfaces? in: S. Osher, N. Paragios (Eds.), Geometric Level Set Methods in Imaging, Vision, and Graphics, Springer, New York, 2003, pp. 381–398.
[7] E. Bänsch, P. Morin, R.H. Nochetto, A finite element method for surface diffusion: the parametric case, J. Comput. Phys. 203 (2005) 321–343.
[8] F. Bornemann, C. Rasch, Finite-Element discretization of static Hamilton–Jacobi equations based on a local variational principle, Comput. Vis. Sci. 9 (2006) 57–69.
[9] M. Burger, Numerical simulation of anisotropic surface diffusion with curvature-dependent energy, J. Comp. Phys. 203 (2005) 602–625.
[10] M. Burger, Finite element approximation of elliptic partial differential equations on implicit surfaces, CAM-Report 05-46, UCLA, 2005.
[11] W.C. Carter, J.W. Cahn, J.E. Taylor, Variational methods for microstructural evolution, JOM 49 (12) (1998) 30–36.
[12] D. Chopp, J.A. Sethian, Motion by intrinsic Laplacian of curvature, Interf. Free Bound. 1 (1999) 107–123.
[13] U. Clarenz, F. Haußer, M. Rumpf, A. Voigt, U. Weikard, On level set formulations for anisotropic fourth order geometric evolution problems, in: A. Voigt (Ed.), Multiscale Modeling in Epitaxial Growth, ISNM 149, Birkhäuser, Basel, 2005, pp. 227–237.
[14] K. Deckelnick, G. Dziuk, A fully discrete numerical scheme for weighted mean curvature flow, Numer. Math. 91 (2002) 423–452.
[15] K. Deckelnick, G. Dziuk, C.M. Elliott, Fully discrete semi-implicit second order splitting for anisotropic surface diffusion of graphs, Preprint, Isaac Newton Institute, Cambridge, 2003.
[16] K. Deckelnick, G. Dziuk, C.M. Elliott, Computation of geometric partial differential equations and mean curvature flow, Acta Numerica (2005) 139–232.
[17] A. DiCarlo, M. Gurtin, P. Podio-Guidugli, A regularized equation for anisotropic motion by curvature, SIAM J. Appl. Math. 52 (1992) 1111–1119.
[18] M. Droske, M. Rumpf, A level set formulation for Willmore flow, Interf. Free Bound. 6 (2004) 361–378.
[19] Q. Du, C. Liu, R. Ryham, X. Wang, A phase field formulation of the Willmore problem, Nonlinearity 18 (2005) 1249–1267.
[20] L.C. Evans, R.F. Gariepy, Measure Theory and Fine Properties of Functions, CRC Press, Boca Raton, FL, 1992.
[21] E. Fried, M.E. Gurtin, A unified treatment of evolving interfaces accounting for small deformations and atomic transport with emphasis on grain-boundaries and epitaxy, Adv. Appl. Mech. 40 (2004) 1–177.
[22] M.B. Giles, N.A. Pierce, An Introduction to the adjoint approach to design, flow, Turb. Comb. 65 (2000) 393–415.
[23] F. Haußer, A. Voigt, A discrete scheme for regularized anisotropic surface diffusion, a sixth order geometric evolution equation, Interf. Free Bound. 7 (2005) 1–17.
[24] F. Haußer, A. Voigt, A discrete scheme for regularized anisotropic curve shortening flow, Appl. Math. Lett. 19 (2006) 691–698.
[25] F. Haußer, A. Voigt, A discrete scheme for parametric anisotropic surface diffusion, J. Sci. Comput., in press.
[26] C. Herring, Some theorems on the free energies of crystal surfaces, Phys. Rev. 82 (1951) 87–93.
[27] M.E. Gurtin, M.E. Jabbour, Interface evolution in three dimensions with curvature-dependent energy and surface diffusion: interface-controlled evolution, phase transitions, epitaxial growth of elastic films, Arch. Rat. Mech. Anal. 163 (2002) 171–208.
[28] F. Liu, H. Metiu, Dynamics of phase separation of crystal surfaces, Phys. Rev. B 48 (1993) 5808.
[29] W.W. Mullins, Two-dimensional motion of idealized grain boundaries, J. Appl. Phys. 27 (1956) 900–904.
[30] W.W. Mullins, Theory of thermal grooving, J. Appl. Phys. 28 (1957) 333–339.
[31] S.J. Osher, R.P. Fedkiw, The Level Set Method and Dynamic Implicit Surfaces, Springer, New York, 2002.
[32] S.J. Osher, J.A. Sethian, Fronts propagating with curvature-dependent speed: algorithms based on Hamilton–Jacobi formulations, J. Comput. Phys. 79 (1988) 12–49.
[33] A. Rätz, A. Ribalta, A. Voigt, Surface evolution of elastically stressed films under deposition by a diffuse interface model, J. Comput. Phys. 214 (2006) 187–208.
[34] A. Rätz, A. Voigt, Higher order regularization of anisotropic geometric evolution equations in three dimensions, J. Comput. Theor. Nanosci. 3 (2006) 560–564.
[35] R.E. Rusu, An algorithm for the elastic flow of surfaces, Interf. Free Bound. 7 (2005) 229–239.
[36] V.A. Shchukin, D. Bimberg, Spontaneous ordering of nanostructures on crystal surfaces, Rev. Mod. Phys. 71 (1999) 1125–1171.
[37] M. Siegel, M.J. Miksis, P.W. Voorhees, Evolution of material voids for highly anisotropic surface energy, J. Mech. Phys. Solids 52 (2004) 1319–1353.

[38] M. Siegert, M. Plischke, Slope selection and coarsening in molecular beam epitaxy, Phys. Rev. Lett. 73 (1994) 1517.
[39] M. Siegert, Coarsening dynamics of crystalline thin films, Phys. Rev. Lett. 81 (1998) 5481.
[40] P. Smereka, Semi-implicit level set methods for curvature and surface diffusion motion, J. Sci. Comp. 19 (2003) 439–456.
[41] B.J. Spencer, Asymptotic solutions for the equilibrium crystal shape with small corner energy regularization, Phys. Rev. E 69 (2004) 011603.
[42] J. Stewart, N.D. Goldenfeld, Spinodal decomposition of a crystal surface, Phys. Rev. A 46 (1992) 6505–6512.
[43] C. Stöcker, S. Vey, A. Voigt, AMDiS – Adaptive multidimensional simulations: composite finite elements and signed distance functions, WSEAS Trans. Circ. Syst. 4 (2005) 111–116.
[44] A. Szczepkowicz, R. Bryl, Observation of vertex-rounding transition for a crystal in equilibrium: oxygen-covered tungsten, Phys. Rev. B 71 (2005) 113416.
[45] Y. Tu, J. Tersoff, Origin of apparent critical thickness for island formation in heteroepitaxy, Phys. Rev. Lett. 93 (2004) 21610.
[46] S. Vey, A. Voigt, AMDiS – adaptive multidimensional simulations: object oriented software concepts for scientific computing, WSEAS Trans. Syst. 3 (2004), 1564–159.
[47] S. Vey, A. Voigt, AMDiS – Adaptive multidimensional simulations, Comp. Vis. Sci., in press.
[48] S.M. Wise, J.S. Lowengrub, J.S. Kim, K. Thornton, P.W. Voorhees, W.C. Johnson, Quantum dot formation on a strain-patterned epitaxial thin film, Appl. Phys. Lett. 87 (2005) 113102.